4

Structure – Property Relationships of Near-Eutectic $BaTiO_3$ – $CoFe_2O_4$ Magnetoelectric Composites

Rashed Adnan Islam[1], Mirza Bichurin[2] and Shashank Priya[3]
[1]*Philips Lumileds Lighting Co, 370 W. Trimble Rd, San Jose CA,*
[2]*Inst. of Electron. & Inf. Syst., Novgorod State Univ., Veliky Novgorod,*
[3]*Materials Science and Engineering, Virginia Tech, Blacksburg, VA 24061,*
[1,3]*USA*
[2]*Russia*

1. Introduction

Magnetoelectric (ME) materials become magnetized when placed in an electric field, and conversely electrically polarized when placed in a magnetic field. Dielectric polarization of a material under magnetic field, or an induced magnetization under an electric field, requires the simultaneous presence of long-range ordering of magnetic moments and electric dipoles (Suchtelen, 1972; Smolensky, 1958; Astrov, 1968; Fiebig 2005). Said materials offer potential for new generations of sensor, filter, and field-tunable microwave dielectric devices (Bichurin, 2002). Unfortunately to date, the ME exchange in single phase materials has been found to be quite small (Dzyaloshinskii, 1959; Astrov, 1960). However, quite large effects are found in composites of piezoelectric and magnetostrictive phases, both of the particle-particle and laminate (Ryu, 2002a, 2002b) types. In these composites, enhanced ME exchange is the result of an elastic-coupling mediated across the piezoelectric-magnetostrictive interfacial area. The original work on ME composites concerned particle-particle composites and was performed at the Philips Laboratories. These ME composites were prepared by unidirectional solidification of an eutectic composition of the quinary system Fe-Co-Ti-Ba-O (O'dell, 1965; Boomgaard, 1976). The eutectic composition was reported to consist of 38 mol% $CoFe_2O_4$. Unidirectional solidification helps in the decomposition of the eutectic liquid (L) into alternate layers of the constituent phases: piezoelectric perovskite (P) and piezomagnetic spinel (S) phases, i.e., $L \rightarrow P + S$. Their results showed ME voltage coefficients as high as dE/dH=50mV/cm•Oe (Boomgaard, 1974; Van Run 1974). Subsequent work on eutectic compositions of $BaTiO_3$-$CoFe_2O_4$ (BTO–CFO) prepared by unidirectional solidification have reported a ME coefficient of 130 mV/cm•Oe (Boomgaard, 1978). Unfortunately, unidirectional solidification has several disadvantages such as (i) limitation on the choice of compositions and material systems, (ii) difficulty in critical control over the composition when one of the components is a gas (i.e., oxygen), and (iii) processing temperature and time. However these limitations could be alleviated by synthesizing ME composites using a conventional ceramic processing route.

Recently, giant ME effect has been reported in laminate composites of piezoelectric and magnetostrictive materials (Ryu, 2003a; Ryu, 2003b; Dong, 2003a; Dong 2003b). The magnetoelectric laminate composite were fabricated in sandwich structure, embedding piezoelectric PMN-PT single crystal between magnetostrictive Terfenol-D alloys. This material exhibited the ME coefficient of 10.30 V/cm.Oe, which is ~80 times higher than that previously reported in either naturally occurring magnetoelectrics or Artificially-Designed Composites (ADC). Even though the ME coefficient is considerably higher, these materials have certain disadvantages as compared with the artificially-designed composites, such as eutectic composition of $BaTiO_3$-$CoFe_2O_4$. Laminated magnetoelectrics are very attractive from the fabrication point of view however suffer from several other drawbacks such as high cost for single crystal, difficult to miniaturize, decay of epoxy bonding and complicated sensing circuits. Again all these laminated composites use lead based product which is a highly toxic element and it is better to eliminate this toxic element and introduce lead-free compositions in magnetoelectric composites.

For bulk magnetoelectric composite higher ME coefficient implies higher elastic coupling between the magnetic and piezoelectric phases (Prellier, 2005). The elastic coupling can be maximized by having coherent response from the magnetostrictive phase under dc bias, so that the stress on the piezoelectric lattice across the grains is in phase with each other. For this purpose, a coherent interface between piezoelectric and magnetostrictive phase is very important. A coherent interface can transfer the strain very efficiently from magnetostrictive to the piezoelectric phase. An artificial interface can also be created by fabricating a co-fired bilayer composite. Previously, we have demonstrated $BaTiO_3$ – $(Ni_{0.8}Zn_{0.2})Fe_2O_4$ bilayer composite having a coherent interface and exhibiting high magnetoelectric sensitivity (Islam, 2006).

In this chapter, high-resolution scanning electron microscopy (SEM) investigation of the product microstructure of BTO–CFO polycrystalline solution that underwent eutectic decomposition has been carried out to compare the interface microstructure with that of co-fired bilayer composites. The interfacial microstructure of said composite was examined, revealing an elemental distribution and grain mismatching between BTO rich grains and a BTO-CFO matrix. Further, we report the magnetoelectric properties of near eutectic compositions. The focus in this study is on quantifying the interface effect rather than magnitude of the magnetoelectric coefficient.

2. Experimental

2.1 Powder preparation and sintering

Reagent-grade powders of $BaCO_3$, TiO_2, $CoCO_3$ and Fe_2O_3, were obtained from Alfa Aesar, Co. MA. USA. Stoichiometric ratios of the powders were mixed according to formulation $BaTiO_3$ (BTO) and $CoFe_2O_4$ (CFO) and ball milled separately for 24 hours with alcohol and YSZ grinding media (5mm diameter, Tosoh Co. Tokyo, Japan). After drying at 80°C the powders were calcined. BTO powders were calcined at 900°C for 3 hours and CFO powders were calcined at 1000°C for 5 hours in separate alumina crucibles. After calcination the powders were crushed and sieved using a sieve of US mesh # 270. After that X-ray diffraction pattern of all different powders (BTO and CFO) were taken to check the formation of single phase perovskite (for BTO) or spinel (for CFO) using Siemens Krystalloflex 810 D500 x-ray diffractometer. Next, 30 and 35 mole% CFO powders were

mixed stoichiometrically with BTO powders. All the powders were mixed using alcohol and grinding media in a polyethylene jar and ball milled for 36 hours. The slurries were dried at 80°C, crushed and sieved with a stainless steel sieve of US mesh #170. The powders were then pressed to pellets of size 12.7x 1.5 mm^2 in a hardened steel die using a hydraulic press under a pressure of 15 MPa. For the bilayer composite, first BTO powders were pressed under 5 MPa pressure and the CFO powders were added on top of BTO powders. These powders were pressed together under 15 MPa pressure. Then the pellets were sealed in a vacuum bag and pressed isostatically in a laboratory cold isostatic press (CIP) under a pressure of 207 MPa. Pressureless sintering of composites was performed in air using a Lindberg BlueM furnace at 1250°C for 5 hours. Bilayer composite was sintered at 1200°C under the same condition. After firing the overall bilayer composite thickness was approximately 1.5 mm with ~1 mm thickness of the CFO and ~0.5 mm thickness of the BTO layer. The diameters of these fired samples were in the range of 10.4 – 10.6 mm.

2.2 Characterization

Microstructural analysis of the sintered samples was conducted by Zeiss Leo Smart SEM using the polished and thermal etched samples. In order to perform magnetoelectric and dielectric measurements, an Ag/Pd electrode was applied on the samples and fired at 850°C for 1 hour. The magnetic properties of the powder and sintered samples were measured by an alternating gradient force magnetometer (AGFM) at room temperature. The magnetoelectric coefficient (dE/dH) was measured by an A.C. magnetic field at 1 kHz and 1 Oe amplitude (H). The AC magnetic field was generated by a Helmholtz coil powered by Agilent 3320 function generator. The output voltage generated from the composite was measured by using a SRS DSP lock- in amplifier (model SR 830). The magnetoelectric coefficient (mV / cm.Oe) was calculated by dividing the measured output voltage by the applied AC magnetic field and the thickness of sample in cm. The sample was kept inside a Helmholtz coil, placed between two big solenoid coils and powered by KEPCO DC power supply. For frequency dependent magnetoelectric coefficient measurement, the Helmholtz coil was powered by the HP 4194 network analyzer (0.5 Oe AC field) and the voltage gain was measured on the secondary terminal. For this measurement, a DC bias of 200 Oe was used using a pair of Sm-Co magnet placed on top and bottom of the sample holder. This set-up produced constant 200 Oe DC bias as measured by the magnetometer. During the frequency dependent measurement, our system was limited to applied DC bias of 200 Oe.

3. Results and discussion

3.1 Structural characterization

Figure 1 (a) shows the X-ray diffraction patterns of calcined BTO and CFO powders. No other phase in addition to perovskite and spinel was detected. The approximate lattice parameter of BTO calculated from the XRD pattern was a = 3.994 Å and c = 4.05 Å where the tetragonality c/a is 1.014. The lattice parameter of CFO powder was calculated to be 8.337Å. Figure 1 (b) shows the composite diffraction pattern of BTO – 30 CFO and BTO – 35 CFO. Only perovskite and spinel peaks were observed in the diffraction pattern. Perovskite peaks are marked as P and spinel peaks are marked as S and the corresponding (hkl) indices are also noted in this figure. It can be seen in this figure that as the percentage of CFO increases, the intensity of perovskite peaks (e.g. P – (101) peak) decreases and the intensity of spinel peak (S – (311)) increases.

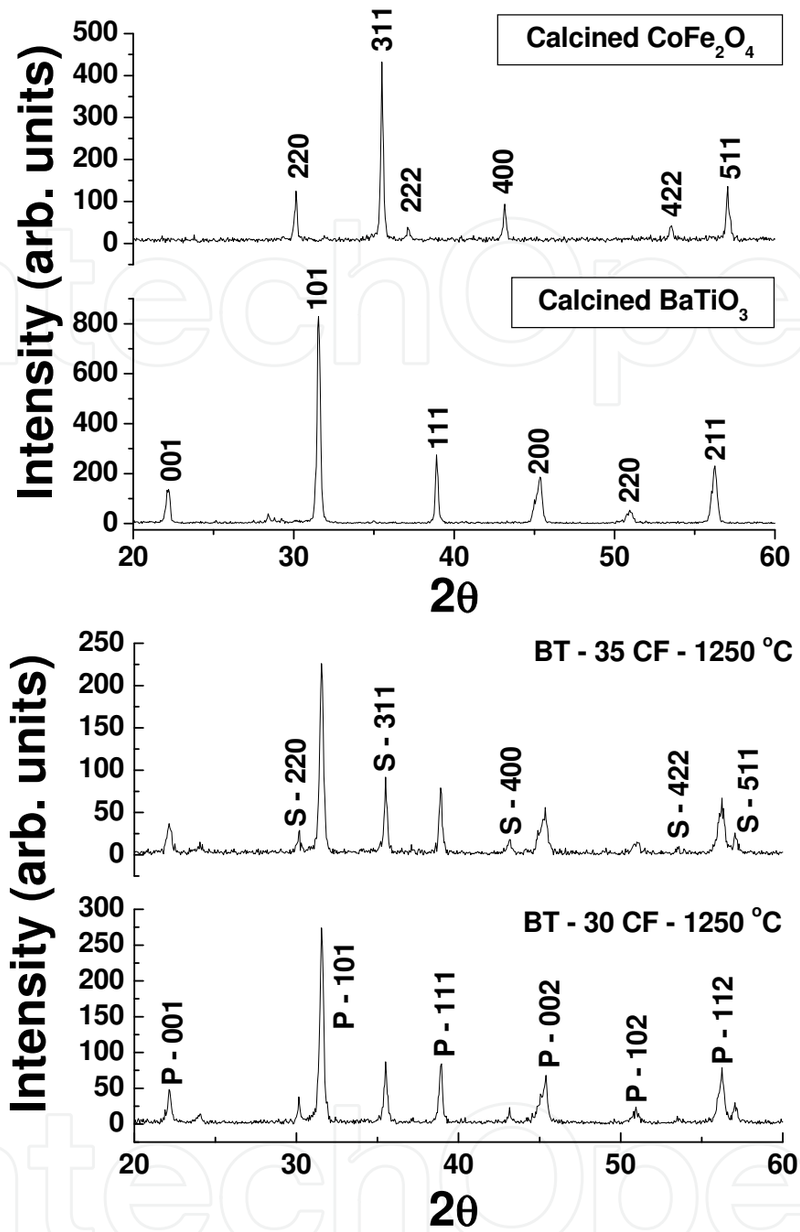

Fig. 1. (a) XRD patterns of calcined BTO and CFO powder and (b) XRD patterns of BT – 30 CF and BT – 35 CF magnetoelectric composite, sintered at 1250°C.

Figure 2 shows the SEM microstructure at low magnification (500X) for (a) BTO–30CFO, and (b) BTO–35CFO. The images reveal island-like structures comprised of multiple grains in a eutectic matrix, as marked in the images. EDS demonstrated that these multi-grain islands were BTO-rich, relative to the matrix that was constituted of a BTO-CFO solution. These microstructural features resemble those of hypo- and/or hyper-eutectic alloys in metallic systems. Some needle-shaped features, as indicated by arrows in Fig. 2 (b), were observed for BTO–35CFO, which were determined to be BTO-rich by EDS. In addition, clear interfaces were observed between the BTO-rich regions and the CFO-rich matrix.

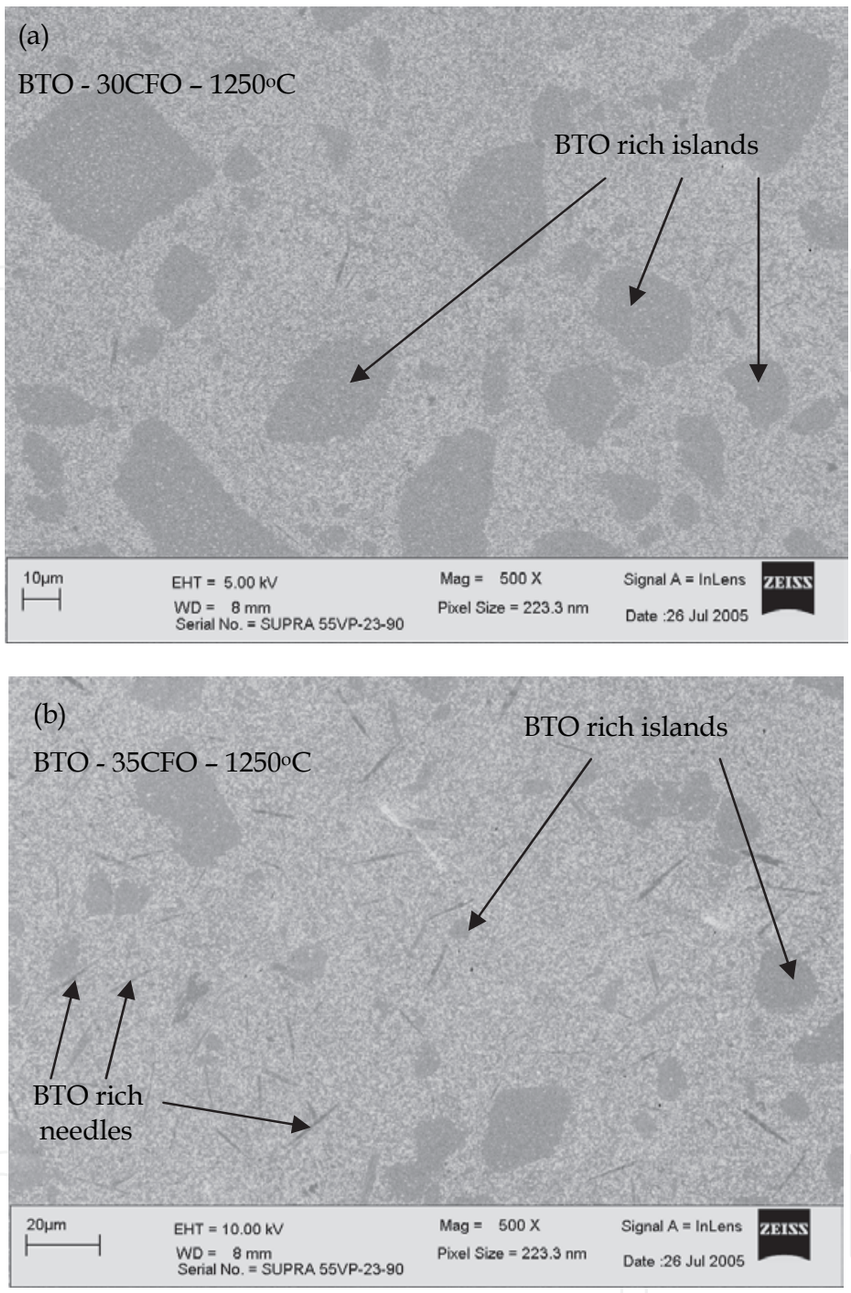

Fig. 2. SEM micrograph of BTO – CFO composites sintered at 1250°C, (Magnification: 500 X). (a). BTO – 30 CFO and (b) BT – 35CFO.

Figure 3(a) is a higher-resolution image showing the grain structure in the vicinity of an interfacial region between the BTO-rich islands and the CFO-rich matrix. A clear boundary between the strained BTO–CFO (i.e., matrix) and BTO-rich (i.e., multi-grain islands) phases is distinguishable, as indicated by dashed line. The deformation of the matrix can be seen by the formation of twin-bands, which reduces the excess strain imposed by the inclusions. Figure 2 also shows magnified (10^5X) images of the microstructure taken from (b) a BTO-rich island, and (c) the CFO-rich matrix. It can be seen that the grain sizes of both regions are

quite small: the average grain size in the BTO-rich islands was ~150nm and that of the CFO-rich matrix region was ~215nm. Due to the formation of $BaTiO_3$ – $CoFe_2O_4$, grain size increased as more $CoFe_2O_4$ and $BaTiO_3$ forms the matrix. Again in the matrix due to the lattice mismatch between $CoFe_2O_4$ (~8.337 Å) and $BaTiO_3$ (a = 3.994 Å and c = 4.05 Å) grain, it is possible to develop stress concentration inside the piezoelectric grain, and the result is presence of twin boundaries, cleavage, strain fields, absence of nanosized domain near the interface and large piezoelectric domain width observed in the matrix. On the other hand the $BaTiO_3$ rich phase has a uniform grain size, lower stress concentration and presence of piezoelectric domains.

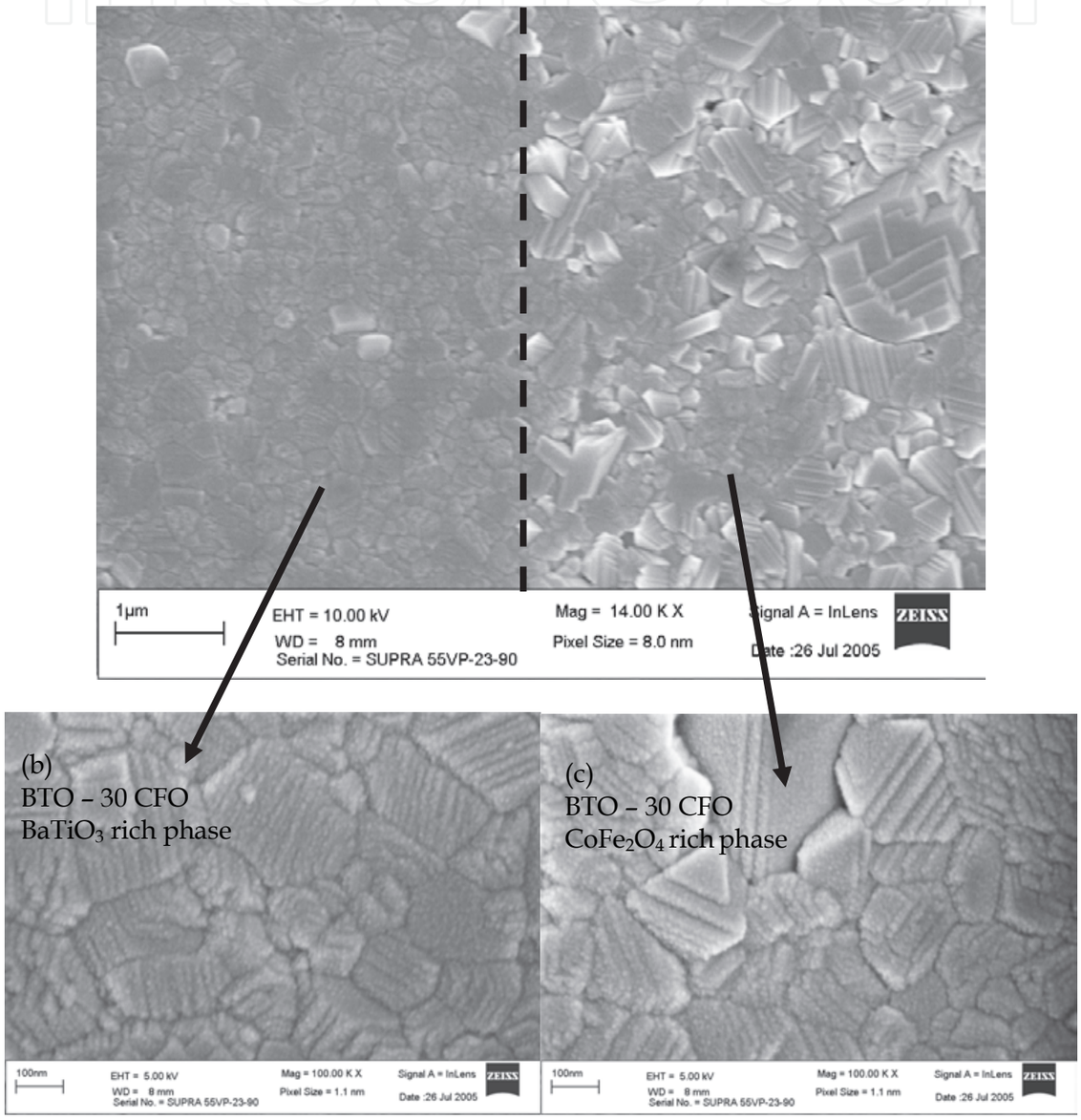

Fig. 3. Magnified SEM image of BTO – CFO magnetoelectric composites at the interface between the BT-rich region and the matrix. (a) interfacial region, (b) grain structure in the BT rich phase (100 kX) and (c) grain structure in the matrix (100 kX).

(a)
BT – 30 CF

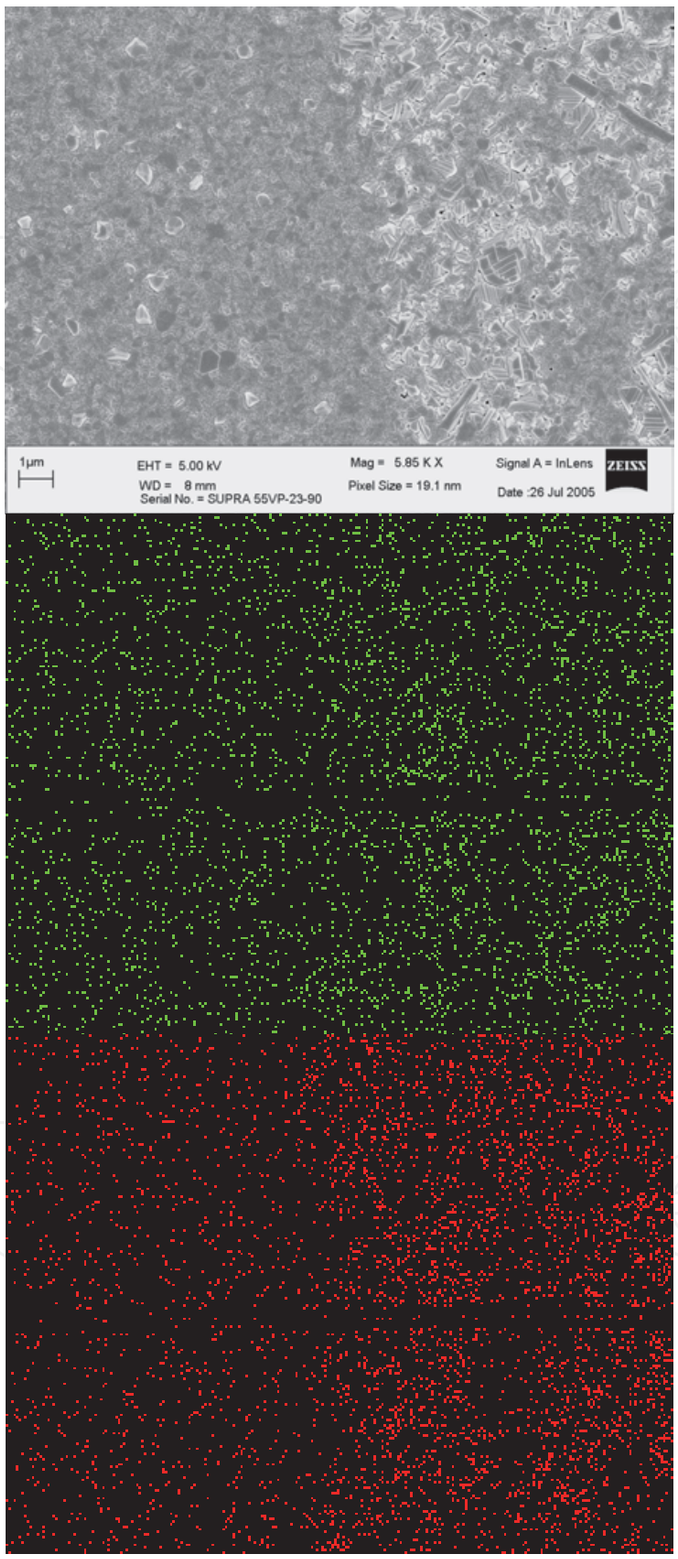

(b)
Co Map

(c)
Fe Map

Fig. 4. Interface microstructure of 0.7 $BaTiO_3$ – 0.3 $CoFe_2O_4$. (a) SEM micrograph, (b) Co distribution and (c) Fe distribution.

Recently, Echigoya et al. have studied the interfacial structure of unidirectional solidified BTO–CFO eutectics, grown by a floating zone method (Echigoya, 2000). Two types of morphologies were found for different growth conditions, and based on HRTEM images the following orientation relationships between phases were identified (a) for hcp $BaTiO_3$: (111)CFO//(00.1)BTO and (110)CFO//(11.0)BTO; and (b) for tetra/cubic $BaTiO_3$: (001)CFO//(001)BTO and (100)CFO//(100) BTO. The results of Fig. 2 show that the polycrystalline ceramics also exhibit high degree of coherency across the interface, evidencing continuous grain growth. X-ray mapping of Co and Fe were done at the interface using Zeiss Leo Smart SEM and it is clearly noticed from the Figure 4 that Co and Fe is rich on the right side of the interface. In the $BaTiO_3$ rich phase, there is a uniform distribution of Co and Fe inside the piezoelectric matrix. EDX elemental analysis shows that, in the $BaTiO_3$ rich phase the atomic percentage of Co and Fe is around 10% and 7% whereas in the matrix, the atomic percentage of Co and Fe raised to 17.76% and 34.73%. These results are consistent with that expected if the BTO-rich regions constitute a hypo-eutectic phase, prior to eutectic decomposition.

Figure 5(a) and (b) shows the bright field TEM images of the sintered BTO – 30 CFO samples. The sintered samples were found to consist of high defect structures such as twin boundaries, cleavage, strain fields etc. in the BTO - CFO matrix which develop to accommodate the mismatch in the BTO and CFO lattices, as CFO lattice parameter is more than double the lattice parameter of BTO lattice. These types of structure usually show larger width domain patterns, characteristic of 90^o domains and the intergranular heterogeneity in domain width is observed. The observed defects are in line with the SEM images. A finer scale domain structure, which usually has striation like morphology and periodically spaced, is almost absent in this structure which means that the structure is in a stressed condition. These finer domains appear when the stress is relieved from the structure.

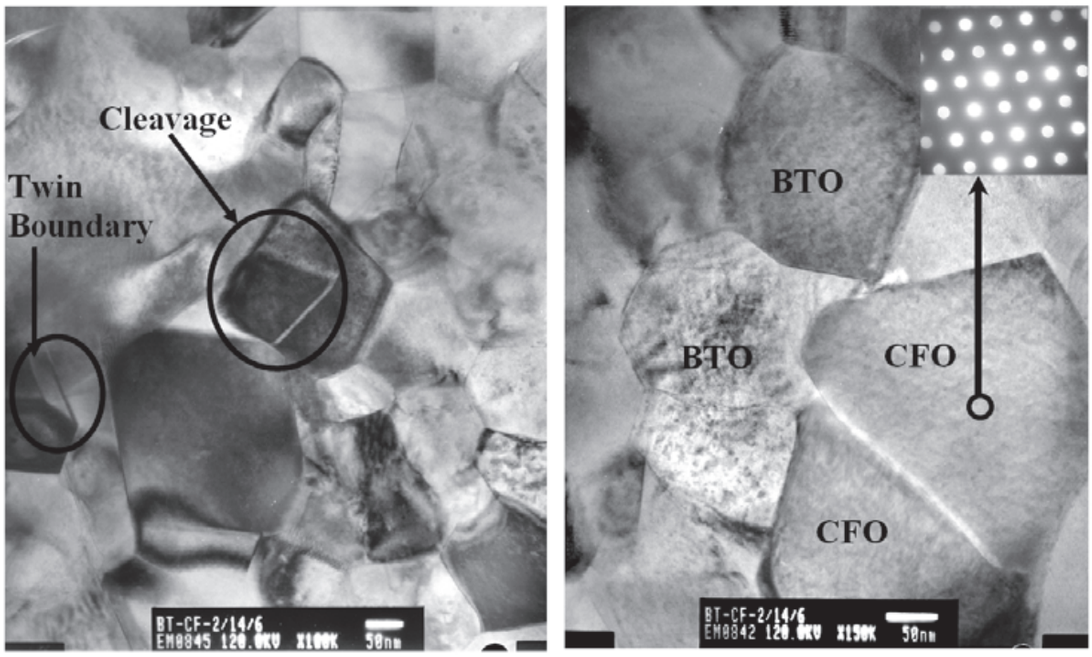

Fig. 5. TEM images of BT – 30 CF composite

Figure 6 shows the interface microstructure of BTO – 33.5 CFO co-fired bilayer composites. A very coherent interface is formed by sintering these two phases together. On the CFO side, an indication of the liquid phase sintering at the interface which may be due to the lower sintering temperature of CFO has been observed. This may be advantageous for accommodating the stress at the interface created in the CFO regions under ac magnetic field. Far from interface, the microstructure observed is single phase on either side.

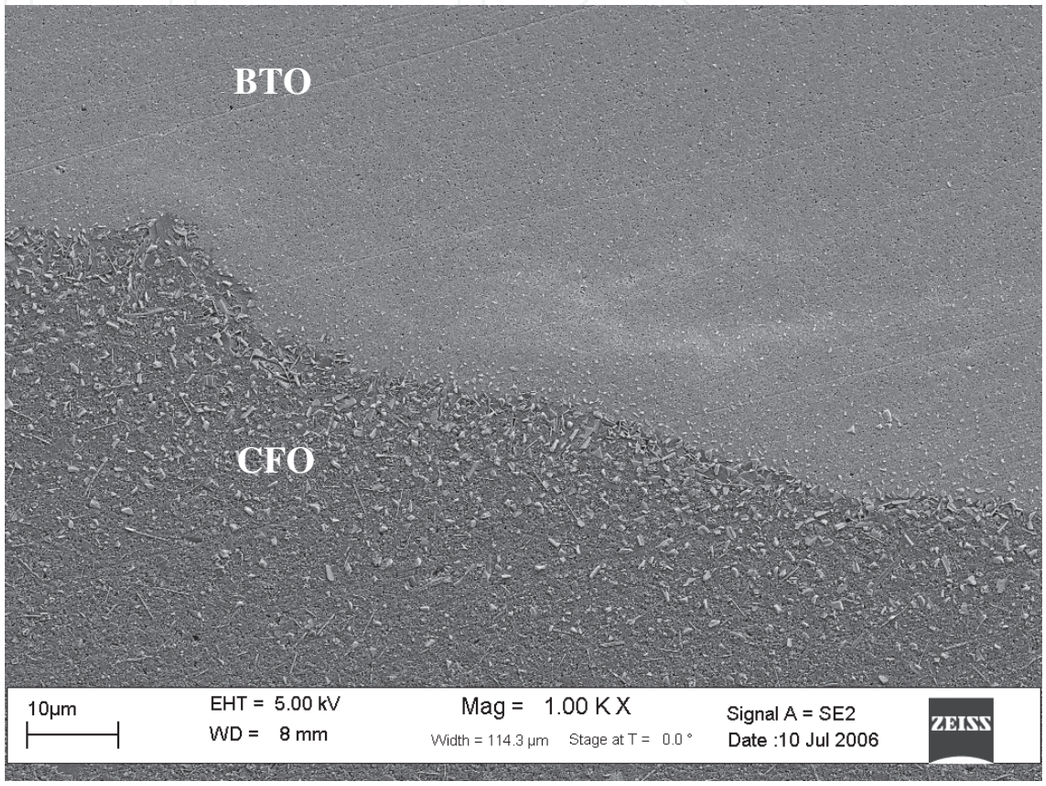

Fig. 6. SEM micrograph of the BTO-CFO bilayer composite.

3.2 Dielectric and ferroelectric characterization

Figure 7 shows the ferroelectric (polarization vs. electric field) and strain (% strain vs. electrical field) of BTO – 33.5 CFO cofired bilayer composite. The polarization of 35 $\mu C/cm^2$ and strain of about 0.14% was recorded at 4.5 kV/mm. Compared to the bilayer composite, the ferroelectric response for the sintered particulate composite was very weak due to the lower resistivity, which clearly indicates the problem in obtaining the larger ME coupling. Interface diffusion and ferrite connectivity reduces the resistivity and hence the decreases the ferroelectric response. Figure 8 (a) to (f) shows the temperature dependence of the dielectric constant and dielectric loss for BT – 30 CFO, BT – 35 CFO and BTO – 33.5 CFO bilayer composites at different frequencies. For bulk (BTO – 30 CFO and BTO – 35 CFO) composites, the maximum in the dielectric constant was found at 145^oC. At 100 Hz frequency, however no peaks were observed in the dielectric loss factor at that temperature as shown in Figure 8 (b) and (d). The sharp increase in the dielectric loss factor was observed for both the compositions at the high temperatures which are related to the space charge effect. A completely different behavior was found when the dielectric

constant and dielectric loss of BTO -33.5 CFO bilayer composite have been plotted in terms of temperature (Figure 8 (e) and (f)). Very sharp peak in dielectric constant was found at around 125 ^{o}C for all of the frequencies (except 100 kHz). This signifies the pure $BaTiO_3$ behavior. Again peaks were observed for dielectric loss at 125 ^{o}C for higher frequencies (10 and 100 KHz). In general BTO - 33.5 CFO bilayer composites found to be a lossy material where the dielectric loss was found to be around 0.4 at 1 kHz and room temperature.

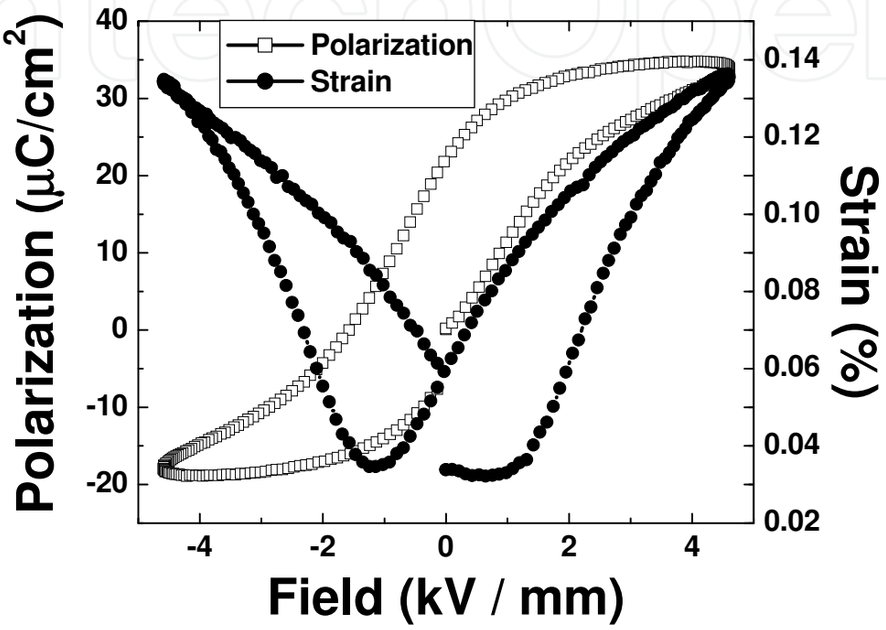

Fig. 7. Ferroelectric properties, polarization and strain as a function of electric field.

3.3 Ferromagnetic and magnetoelectric characterization

Figure 9 shows the magnetic properties for sintered BT – 30 CFO, BT – 35CFO and BTO – 33.5 CFO cofired bilayer composite. The co-fired bilayer composite shows higher saturation (0.881 emu) magnetization and slightly higher coercive field (973.33 Oe) than BTO – CFO bulk composite. BTO – 35 CFO shows saturation magnetization of 0.881 emu and coercivity of 973.33 Oe as indicated in Table 1. This is due to the contribution of pure CFO phase. Bilayer composite also shows better remnant magnetization than the bulk. Figure 10 (a) shows the variation of magnetoelectric coefficient as a function of dc bias. The bulk composites show the maxima at 1500 Oe with a ME coefficient of 2.2 mV/cm. Oe for BTO – 35 CFO. But for the bilayer composite it reaches a maximum value of 3.9 mV/cm.Oe and then saturates. The measurement has been taken in condition where the applied magnetic field is perpendicular to the sample surface. Figure 10 (b) shows the frequency dependent magnetoelectric coefficient. At around 430 kHz all the samples show giant magnetoelectric coefficient. BTO – 33.5 CFO bilayer composite exhibits ME coefficient around 3.6 V/cm.Oe and the BTO – 35 CFO bulk composite reaches around 0.95 V/cm. Oe. This is a very high magnetoelectric coefficient for BTO – CFO composite at resonance frequency, which is higher than the recent reported value of 2540 mV/cm.Oe at 160 KHz and 270 Oe DC bias for BTO – 20 CFO composite (Ren, 2005).

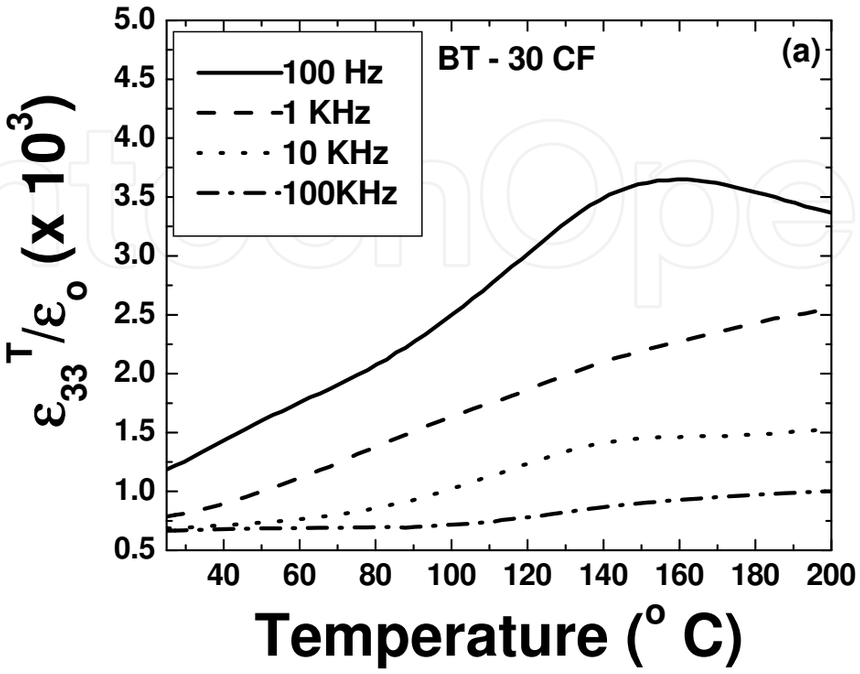
100 Hz
1 KHz
10 KHz
100KHz
BT - 30 CF
(a)
$\varepsilon_{33}^{T}/\varepsilon_o$ (x 10^3)
Temperature (^{o} C)

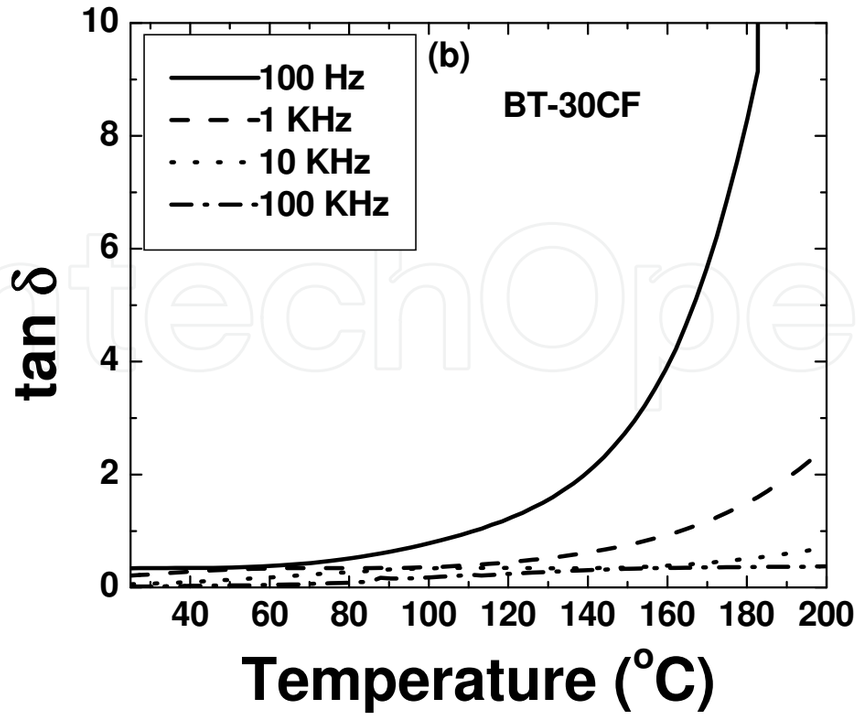
100 Hz
1 KHz
10 KHz
100 KHz
(b)
BT-30CF
tan δ
Temperature (^{o}C)

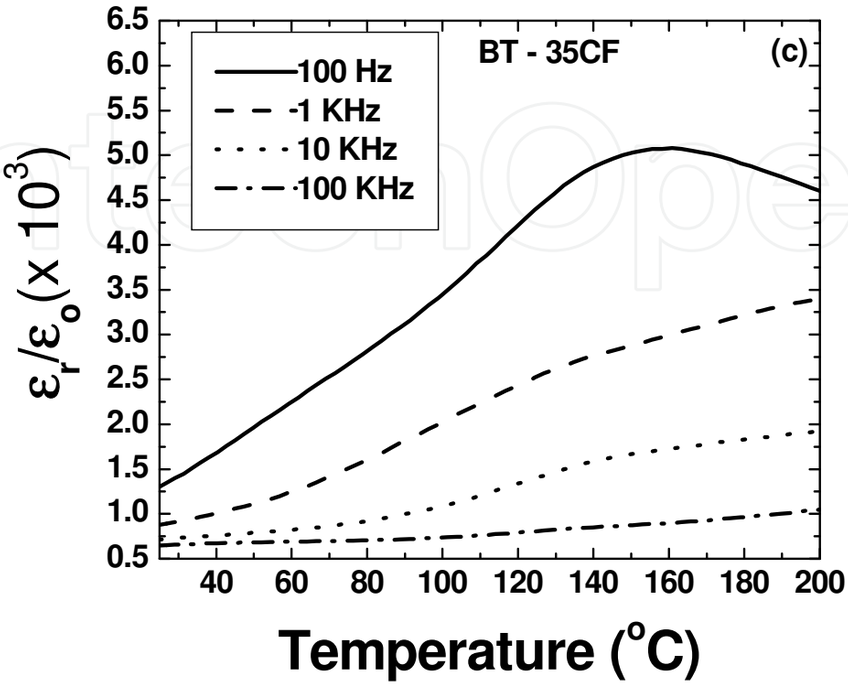
BT - 35CF
(c)
100 Hz
1 KHz
10 KHz
100 KHz
$\varepsilon_r/\varepsilon_o$ (x 10^3)
Temperature (^{o}C)

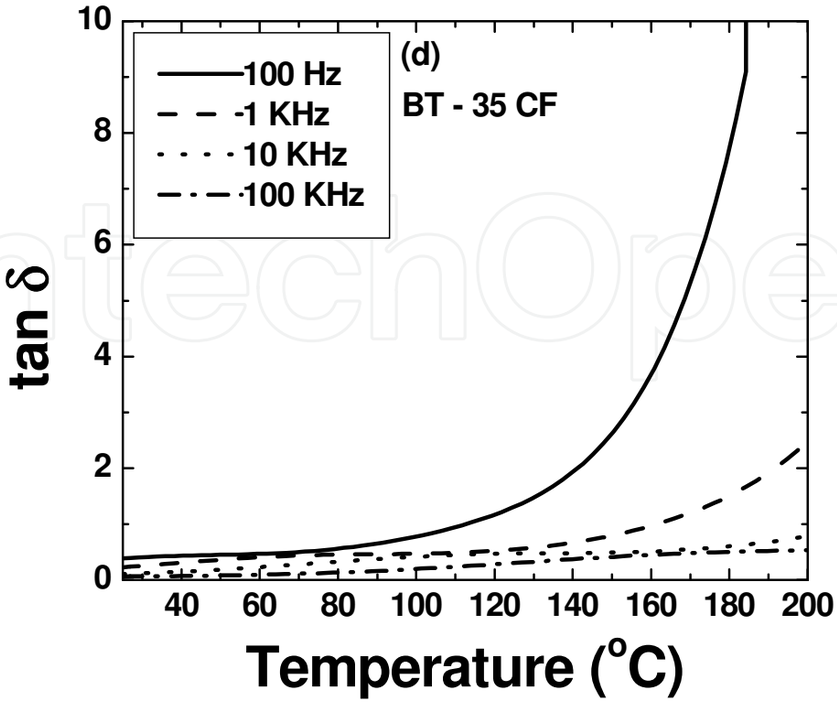
(d)
BT - 35 CF
100 Hz
1 KHz
10 KHz
100 KHz
tan δ
Temperature (^{o}C)

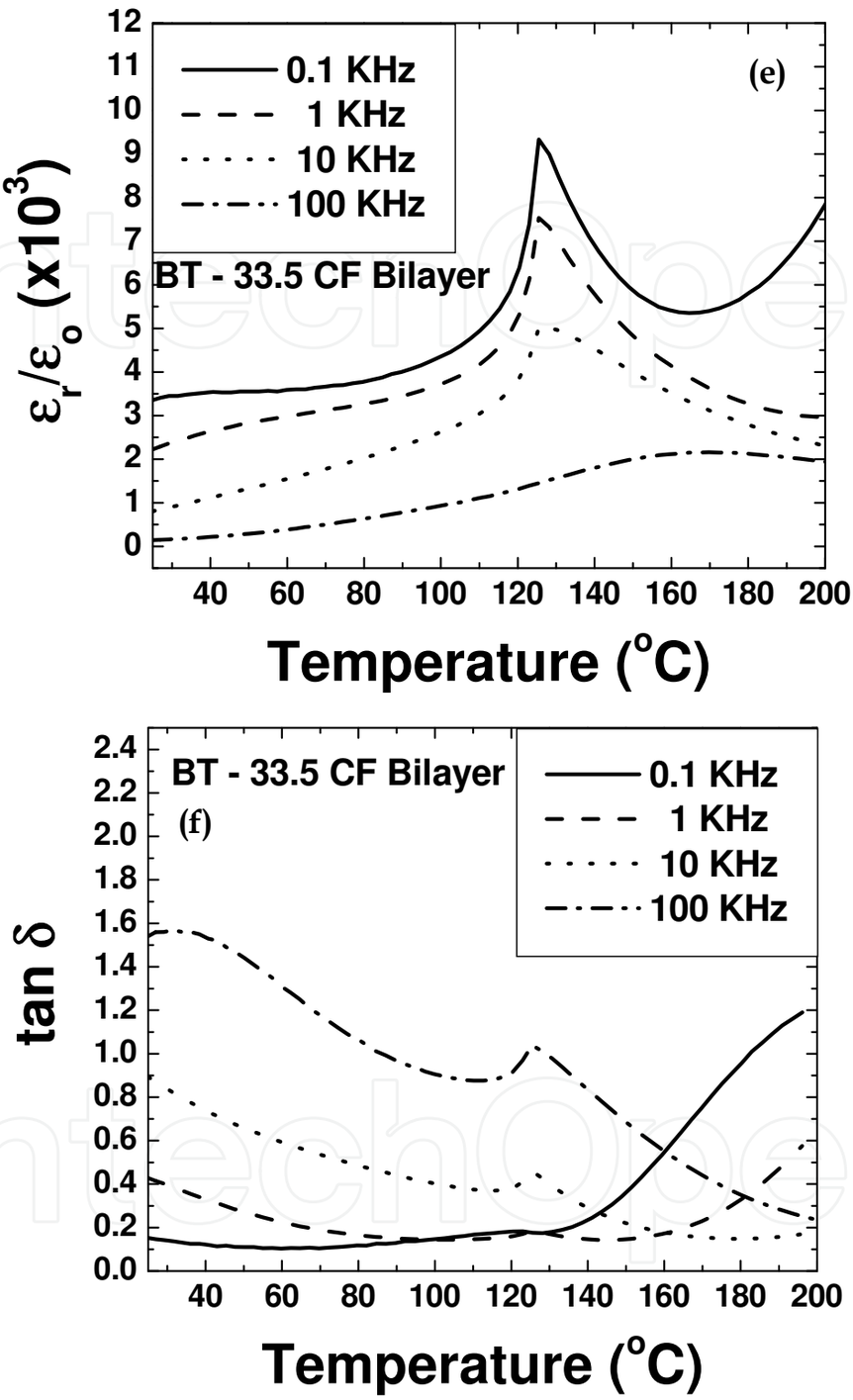

Fig. 8. Dielectric properties of BTO – CFO composites, (a) temperature dependent dielectric constant for BTO – 30 CFO, (b) temperature dependent dielectric loss for BTO – 30 CFO, (c) temperature dependent dielectric constant for BTO – 35 CFO, (d) temperature dependent dielectric loss for BTO – 35 CFO, (e) temperature dependent dielectric constant for BTO – 33.5 CFO and (f) temperature dependent loss constant for BTO – 33.5 CFO.

Analysis of low frequency ME effect in the layered CFO-BTO structures (Fig.10 (a)) can be conducted based on the equation for the longitudinal ME coefficient (Bichurin, 2003):

$$\alpha_{E,33}=\frac{E_3}{H_3}=2\frac{\mu_0 kv(1-v)\,{}^{p}d_{31}\,{}^{m}q_{31}}{\{2\,{}^{p}d_{31}^2(1-v)+{}^{p}\varepsilon_{33}[({}^{p}s_{11}+{}^{p}s_{12})(v-1)-v({}^{m}s_{11}+{}^{m}s_{12})]\}}\times$$
$$\times\frac{[({}^{p}s_{11}+{}^{p}s_{12})(v-1)-kv({}^{m}s_{11}+{}^{m}s_{12})]}{\{[\mu_0(v-1)-{}^{m}\mu_{33}v][kv({}^{m}s_{12}+{}^{m}s_{11})-({}^{p}s_{11}+{}^{p}s_{12})(v-1)]+2\,{}^{m}q_{31}^2kv^2\}}$$

The equation presented above allows for the determination of the longitudinal ME coefficient as function of volume fractions, physical parameters of phases and elastic-elastic interfacial coupling parameter k. From comparison of theory and data the importance of an interfacial coupling parameter between phases can be inferred. This interphase interfacial connection parameter was shown to be weak for CFO–BTO. In our case k is about 0.1. Estimation of ME effect in the EMR range (Fig.10(b)) has been performed using the above equation (Bichurin, 2003). Because of inconveniences in the analytical expressions for effective parameters of bulk CFO-BTO composites, computer calculations of the dependence of effective parameters on the relative piezoelectric phase volume in ME composite have been performed. Calculations of longitudinal ME coefficient have also been performed for electric and magnetic fields applied for bulk composites using the material parameters in (Harshe, 1993; Bichurin, 2010). The obtained values of the ME voltage coefficient coincide with previously published data. As follows from the comparison of obtained results, the ME voltage coefficient was approximately 20% greater than that calculated from the experimental data using the model. This is explained by the fact that the internal (local) magnetic field in the ferrite component is considerably different than that of the externally applied magnetic field.

	BTO – 30 CFO	**BTO – 35 CFO**	**BTO -33.5 CFO**
Coercivity (Oe)	646.77	677.49	973.3
Saturation magnetization (emu/ 100 gm)	0.557	0.702	0.881
Remnant magnetization (emu/ 100 gm)	0.246	0.279	0.345

Table 1. Magnetic Properties of BTO – CFO Composites

This question of 'why the elastic interaction in system with uniform distribution of two phases and coherent interfaces between the phases is weak' needs addressing. Our results indicate that the reasons for weak response may not be related to elastic-coupling between phases, but rather to the magnetic flux distribution within the matrix. Compared to the results of Philips Research Lab, the 1 kHz values reported here are quite low, which can be attributed to the process difference, polycrystalline matrix, nanograin structure and twin formation. In our research we used conventional sintering method compared to the unidirectional solidification of Philips Laboratory. In unidirectional solidification process, a significant amount of time is allowed to melt the components under desired atmosphere and then solidify with heat transfer confined along one direction. This results in the consolidation of the ferrite into dendrite structure, which hinders the distribution of the ferrite phases. Also the longer time helps the grain growth and unidirectional solidification

results in preferential texture. All these contributes to the larger ME coefficient. In our process smaller grain size (150 – 215 nm) results in lower ME coefficient and also the well dispersed ferrite particle reduces the resistivity of the overall bulk composite system. Grain size has significant effect on the magnitude of ME coefficient. Our previous results show that as the piezoelectric grain size drops below 200 nm, the ME coefficient drops rapidly (Islam, 2008). Finally in conventional sintering the grains are in random orientations and defects (such as twin boundaries, cleavage) in the structures are notable, all of which hinder the piezoelectric properties. The ME coefficient was notably higher for the bilayer, than for the eutectic composites. This comparison shows that coherent interfaces between composites of similar composition is not by any means the factor controlling the magnitude of the ME coefficient. Rather, continuity of flux lines is equally important for the expression of the ME product tensor property between phases.

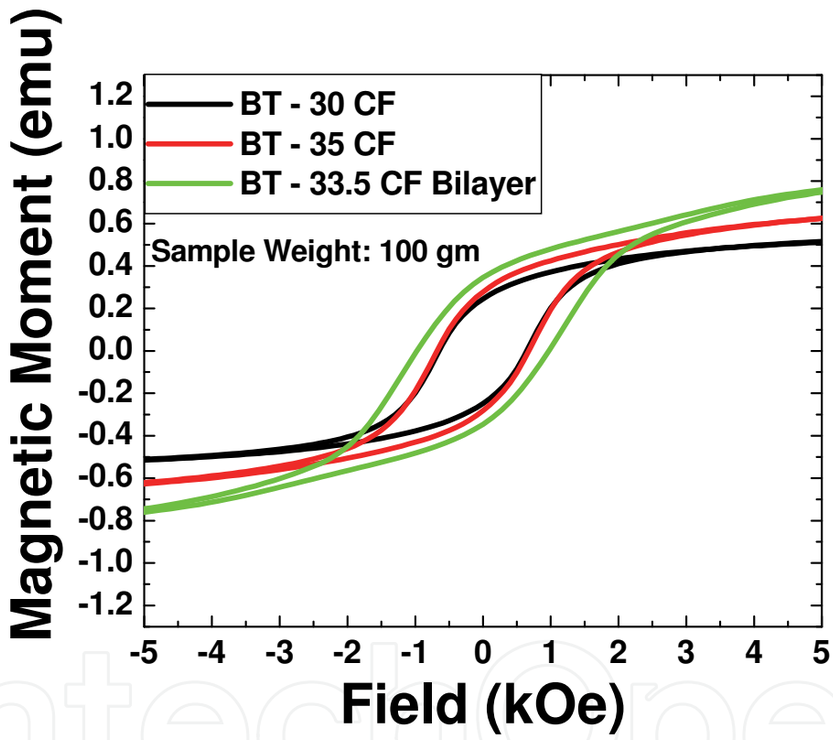

Fig. 9. Ferromagnetic Hysteresis loop of sintered BTO – 30 CFO, BTO – 35 CFO and BTO – 33.5 CFO bilayer magnetoelectric composites.

4. Conclusion

A microstructural investigation of $BaTiO_3$–$CoFe_2O_4$ polycrystalline solutions for compositions close to the eutectic point has been investigated along with dielectric, ferromagnetic and magnetoelectric behavior. Multi-grain BTO-rich islands were found in a CFO-rich matrix. Analysis of the interfacial regions revealed that the two phases have a high degree of coherency, enabling continuous grain growth. Also the bilayer type composite structure shows better performance as it shows very high magnetoelectric coefficient (3.6 V/cm. Oe) at high frequency (434 KHz).

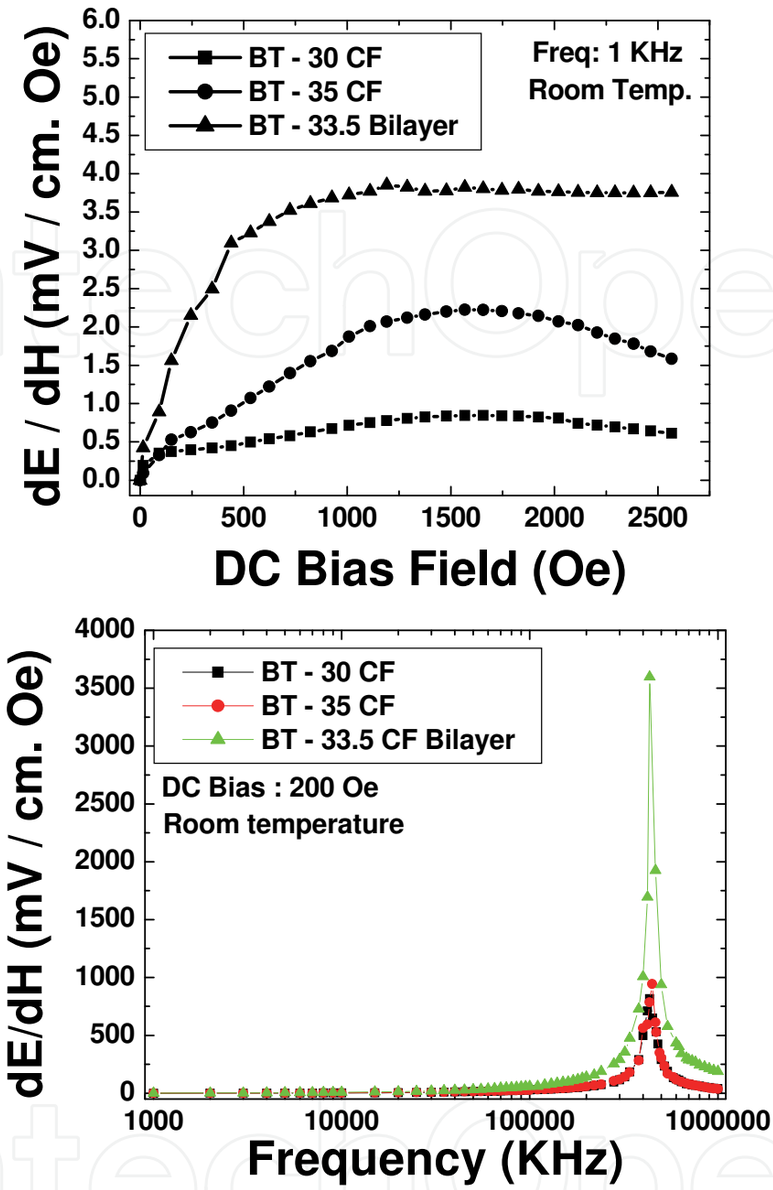

Fig. 10. Magnetoelectric Coefficient of different BTO – CFO composites as a function of (a) DC bias and (b) frequency.

5. Acknowledgement

The authors gratefully acknowledge the support from National Science Foundation INAMM program.

6. References

Astrov, DN. Al'shin, BI. Zhorin, RV. and Drobyshev, LA. (1968). *Sov. Phys. – JETP 28.* pp. 1123.

Astrov DN. (1960). *Sov. Phys. – JETP*, 11, pp. 708.

Bichurin, MI, Petrov, VM, Petrov, RV. et. al. (2002). Magnetoelectric microwave devices. *Ferroelectrics*, 280, 211.

Bichurin MI, Petrov VM, Srinivasan G. (2003) Theory of low-frequency magnetoelectric coupling in magnetostrictive-piezoelectric bilayers. *Phys. Rev.*, B68, pp. 054402.

Bichurin MI, Filippov DA, Petrov VM et al. (2003) Resonance magnetoelectric effects in layered magnetostrictive-piezoelectric composites *Phys.Rev*. B68, pp. 132408.

Bichurin MI, Petrov VM, Averkin SV, Filippov AV. (2010) Electromechanical resonance in magnetoelectric layered structures. *Physics of the Solid State*, 52, pp. 2116-2122.

Boomgaard JVD, Van Run AMJG and Suchtelen JV. (1976). Magnetoelectricity in Piezoelectric – Magnetostrictive Composite. *Ferroelectrics.* 10. pp. 295-298.

Boomgaard JVD and Born RAJ. (1978). A Sintered Magnetoelectric Composite Material $BaTiO_3$- Ni (Co, Mn) Fe_2O_4. J.Mater.Sci. 13. pp. 1538-1548.

Boomgaard JVD, Terrell DR, Born RAJ et. al. (1974) An insitu grown Eutectic Magnetoelectric Composite Material: Part I: Composition and Unidirectional Solidification. *J.Mater.Sci.* 9. pp. 1705-1709.

Dong S, Li J, and Viehland, D. (2003). Ultrahigh Magnetic Field Sensitivity in Laminates of Terfenol-D and $Pb(Mg_{1/3}Nb_{2/3})O_3$-$PbTiO_3$. *Appl. Phys. Lett.*; 83 [11]. pp. 2265-2267.

Dong S, Li J, and Viehland D (2003). Giant Magnetoelectric Effect in Laminate Composite. IEEE Trans. Ultrason. Ferroelec. Freq. Ctrl., 50 [10], pp. 1236-1239.

Dzyaloshinskii, IE. (1959). On the magneto-electrical effects in antiferromagnets. *Sov. Phys. JETP*. 10. pp. 628–629.

Echigoya J, Hayashi S and Obi Y. (2000) Directional solidification and interface structure of $BaTiO_3$-$CoFe_2O_4$ eutectic, *J. Mater. Sci.*, 35, pp 5587.

Feibig, M. (2005). Revival of Magnetoelectric Effect. *J.Phys. D: Appl. Phys.;* 38, pp. R123-R152.

Harshe G, Dougherty JP, Newnham RE. (1993). Theoretical modeling of multilayer magnetoelectric composites, *Int. J. Appl. Electromagn. Mater.,* 4, pp. 161.

Islam RA and Priya S. (2006). Magnetoelectric properties of the lead--free cofired $BaTiO_3$-$Ni_{0.8}Zn_{0.2}Fe_2O_4$ bilayer composite. *Appl. Phys. Lett,* 89, 152911.

Islam RA and Priya S. (2008), Effect of piezoelectric grain size on magnetoelectric coefficient of $Pb(Zr_{0.52}Ti_{0.48})O_3$-$Ni_{0.8}Zn_{0.2}Fe_2O_4$ particulate composites *J. of Mater. Sci.,* 43 (10), pp. 3560.

O'dell TH. (1965). Magnetoelectrics – A New Class of Materials. *Electronics and Power*. 11. pp. 266-268.

Prellier W, Singh MP and Murugavel P. (2005). The single-phase multiferroic oxides: from bulk to thin film *J. Phys: Condensed Matter.,* 17, R803.

Ren SQ, Weng LQ, Song SH et. al. (2005) $BaTiO_3$/$CoFe_2O_4$ particulate composites with large high frequency magnetoelectric response *J. Mater. Sci.* 40, pp. 4375.

Ryu J, Priya S and Uchino K. (2002). Magnetoelectric Effect in Composites of Magnetostrictive and Piezoelectric Materials. *J. Electroceram*. 8, pp. 107- 119.

Ryu J, Priya S, Uchino K, Viehland D et. al. (2002). High Magnetoelectric Properties in $0.68Pb(Mg_{1/3}Nb_{2/3})O_3$-$0.32PbTiO_3$ Single Crystal and Terfenol-D Laminate Composite. *J. Korean Ceram. Soc.* 39. pp. 813-817.

Ryu, J, Priya, S, Carazo, AV et. al. (2001). Effect of the Magnetostrictive Layer on Magnetoelectric Properties in Lead Zirconate Titanate/Terfenol-D Laminate Composites, J. of Amer. Ceram. Soc. 84 (12). pp. 2905 – 2908.

Ryu J, Carazo AV, Uchino K, et. al. Piezoelectric and Magnetoelectric Properties of Lead Zirconate Titanate/Ni-Ferrite Particulate Composites. *J. of Mater. Sci.* 7 (1). pp. 17 – 24.

Smolensky, G. and Ioffe, VA. (1958). *Colloque International du Magnetisme*; Communication No. 71.

Suchtelen, JV. (1972). Product Properties: A New Application of Composite Materials. *Philips Research Report*, 27, pp. 28 – 37.

Van Run AMJG, Terrell DR, and Scholing JH. (1974) An insitu grown Eutectic Magnetoelectric Composite Material.

Magnetoelectric Composite Material. Part II: Physical Properties. *J.Mater.Sci.* 9. pp 1710 - 1714.

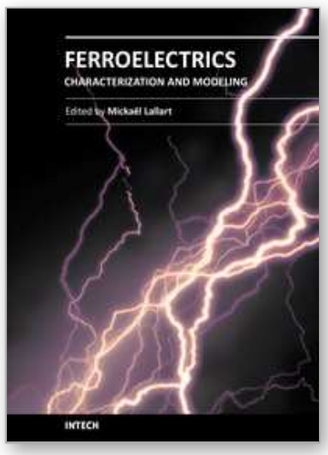

Ferroelectrics - Characterization and Modeling

Edited by Dr. MickaÃ«l Lallart

ISBN 978-953-307-455-9
Hard cover, 586 pages
Publisher InTech
Published online 23, August, 2011
Published in print edition August, 2011

Ferroelectric materials have been and still are widely used in many applications, that have moved from sonar towards breakthrough technologies such as memories or optical devices. This book is a part of a four volume collection (covering material aspects, physical effects, characterization and modeling, and applications) and focuses on the characterization of ferroelectric materials, including structural, electrical and multiphysic aspects, as well as innovative techniques for modeling and predicting the performance of these devices using phenomenological approaches and nonlinear methods. Hence, the aim of this book is to provide an up-to-date review of recent scientific findings and recent advances in the field of ferroelectric system characterization and modeling, allowing a deep understanding of ferroelectricity.

InTech Europe
University Campus STeP Ri
Slavka Krautzeka 83/A
51000 Rijeka, Croatia
Phone: +385 (51) 770 447
Fax: +385 (51) 686 166
www.intechopen.com

InTech China
Unit 405, Office Block, Hotel Equatorial Shanghai
No.65, Yan An Road (West), Shanghai, 200040, China
中国上海市延安西路65号上海国际贵都大饭店办公楼405单元
Phone: +86-21-62489820
Fax: +86-21-62489821

IntechOpen